

## Supplementary data

**Title: Combined use of quantitative ED-EPMA, Raman microspectrometry, and ATR-FTIR imaging techniques for the analysis of individual particles**

Authors: Hae-Jin Jung<sup>1</sup>, Hyo-Jin Eom<sup>1</sup>, Hyun-Woo Kang<sup>1</sup>, Myriam Moreau<sup>2</sup>, Sophie Sobanska<sup>2</sup>, and Chul-Un Ro<sup>1,\*</sup>

<sup>1</sup> Department of Chemistry, Inha University, Yonghyun Dong, Nam Gu, 402-751, Incheon, South Korea

<sup>2</sup> Laboratoire de Spectrochimie Infrarouge et Raman, UMR CNRS 8516, Université de Lille 1, Bât. C5, 59655 Villeneuve d'Ascq Cedex, France

### **A summary of the supporting information:**

Tables S1 and Figures S1-S13

**Table S1.** Raman and ATR-FTIR peaks of observed chemical species.

<b>Chemical species</b>	<b>Raman and IR peaks (in cm<sup>-1</sup>)[ref.]</b>	
<b>Anhydrite</b>	<b>Raman peaks [1]</b>	415, 497, 608, 626, 675, 1016, 1111, 1128, 1160
	<b>ATR-FTIR peaks [2]</b>	1133, 1096, 1016
<b>Gypsum</b>	<b>Raman peaks [3]</b>	415, 494, 620, 670, 1008, 1136
	<b>ATR-FTIR peaks [2]</b>	3505, 3400, 1682, 1618, 1104, 1004
<b>Calcite</b>	<b>Raman peaks [4]</b>	282, 713, 1087, 1437, 1748
	<b>ATR-FTIR peaks [2]</b>	1792, 1392, 866, 709
<b>Quartz</b>	<b>Raman peaks [5]</b>	128, 206, 264, 355, 394, 401, 464, 697, 807, 1161
	<b>ATR-FTIR peaks [2]</b>	1162, 1057, 796, 777
<b>Sodium sulfate</b>	<b>Raman peaks [6]</b>	450, 466, 620, 632, 647, 993, 1101, 1131, 1152
	<b>ATR-FTIR peaks [7]</b>	1102
<b>Sodium nitrate</b>	<b>Raman peaks [8]</b>	724, 1068, 1385
	<b>IR peaks [9]</b>	1789, 1349, 834
<b>K-feldspar</b>	<b>Raman peaks [10]</b>	256, 265, 286, 332, 373, 403, 452, 475, 513, 585, 651, 749, 813, 993, 1124, 1137
	<b>ATR-FTIR peaks [2]</b>	1133, 1048, 1006, 771, 727

## References

1. Ma, Y.; Zhou, Q.; He, Z.; Li, F.; Yang, K.; Cui, Q.; Zou, G. High-pressure and high-temperature study of the phase transition in anhydrite. *J. Phys.: Condens. Matter.* **2007**, *19*, 425221.

2. Jung, H.-J.; Malek, M.A.; Ryu, J.; Kim, B.; Song, Y.-C.; Kim, H.; Ro, C.-U. Speciation of Individual Mineral Particles of Micrometer Size by the Combined Use of Attenuated Total Reflectance-Fourier Transform-Infrared Imaging and Quantitative Energy-Dispersive Electron Probe X-ray Microanalysis Techniques. *Anal. Chem.* **2010**, *82*, 6193-6202.
3. Knittle, E.; Phillips, W.; Williams, Q. An infrared and Raman spectroscopic study of gypsum at high pressures. *Phys. Chem. Minerals.* **2001**, *28*, 630-640.
4. Gunasekaran, S.; Anbalagan, G.; Pandi, S. Raman and infrared spectra of carbonates of calcite structure. *J. Raman Spectrosc.* **2006**, *37*, 892-899.
5. Kingma, K.; Hemley, R. Raman spectroscopic study of microcrystalline silica. *Am. Mineral.* **1994**, *79*, 269-273.
6. Dong, J.-L.; Xiao, H.-S.; Zhao, L.-J.; Zhang, Y.-H. Spatially resolved Raman investigation on phase separations of mixed Na<sub>2</sub>SO<sub>4</sub>/MgSO<sub>4</sub> droplets. *J. Raman Spectrosc.* **2009**, *40*, 338–343.
7. Miller, F. A.; Wilkins, C. H. Infrared Spectra and Characteristic Frequencies of Inorganic Ions. *Anal. Chem.* **1952**, *24*, 1253-1294.
8. Rousseau, D.; Miller, R.; Leroi, G. Raman spectrum of crystalline sodium nitrate. *J. Chem. Phys.* **1968**, *48*, 3409-3413.
9. Ryu, J.; Ro, C.-U. Attenuated total reflectance FT-IR imaging and quantitative energy dispersive-electron probe X-ray microanalysis techniques for single particle analysis of atmospheric aerosol particles. *Anal. Chem.* **2009**, *81*, 6695-6707.
10. Freeman, J.; Wang, A.; Kuebler, K.; Jolliff, B.; Haskin, L. CHARACTERIZATION OF NATURAL FELDSPARS BY RAMAN SPECTROSCOPY FOR FUTURE PLANETARY EXPLORATION. *Can. Mineral.* **2008**, *46*, 1477-1500.

**Figure S1.** (A) Secondary electron image (SEI) from SEM before ATR-FTIR measurement, (B) optical image from Raman spectrometer, (C) ATR-FTIR image at  $1100\text{ cm}^{-1}$ , and (D) SEI after ATR-FTIR measurement of the same 12 gypsum particles on Al foil.

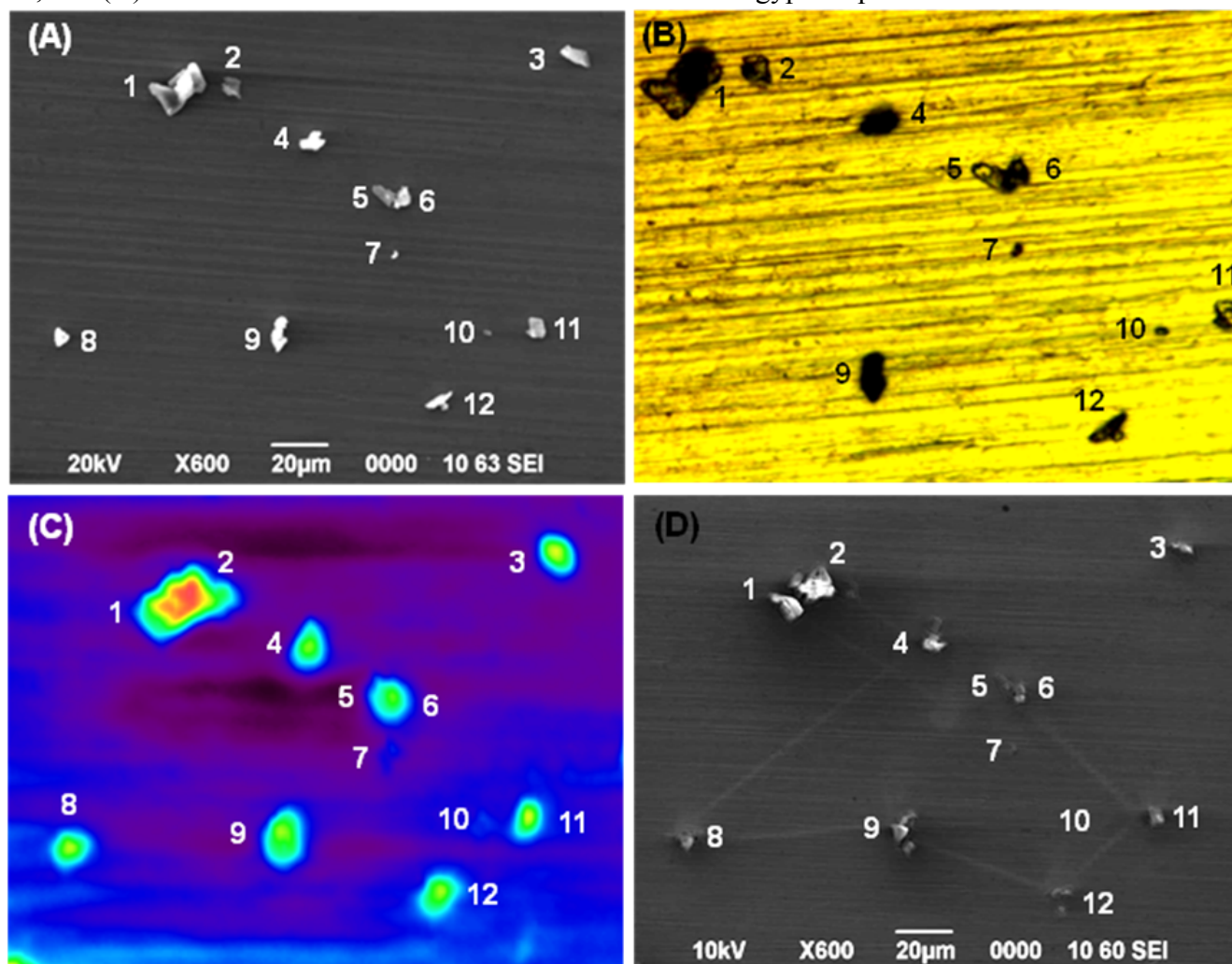


**Figure S2.** (A) SEI from SEM before ATR-FTIR measurement, (B) optical image from Raman spectrometer, (C) ATR-FTIR image at  $1390\text{ cm}^{-1}$ , and (D) SEI after ATR-FTIR measurement of the same 15 calcite particles on Ag foil.

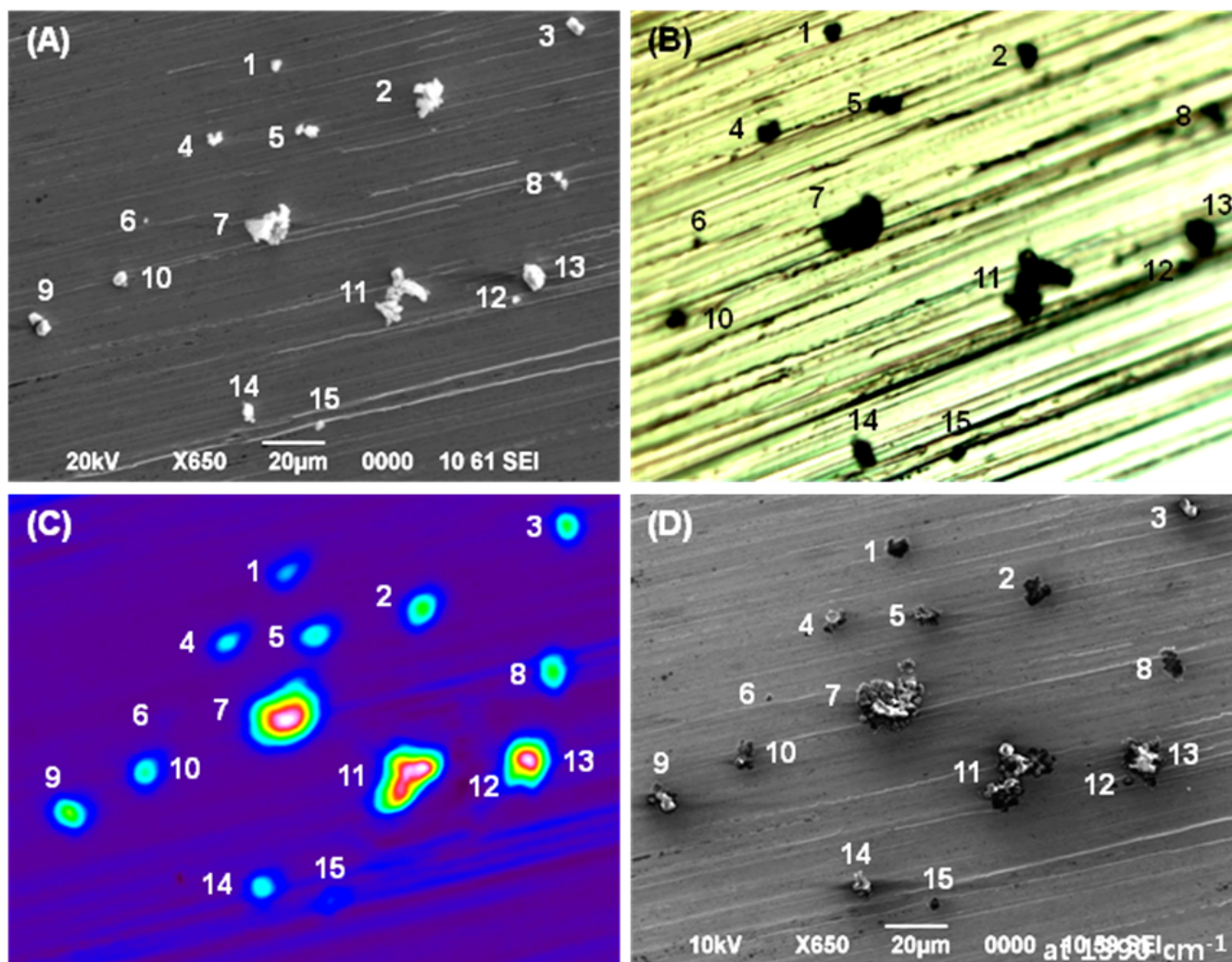


**Figure S3.** (A1) Optical image from Raman spectrometer, (A2) corresponding Raman image, and (A3) SEI of calcite particle #13, respectively, and (B) its X-ray spectrum, (C) Raman spectrum, and (D) ATR-FTIR spectrum.

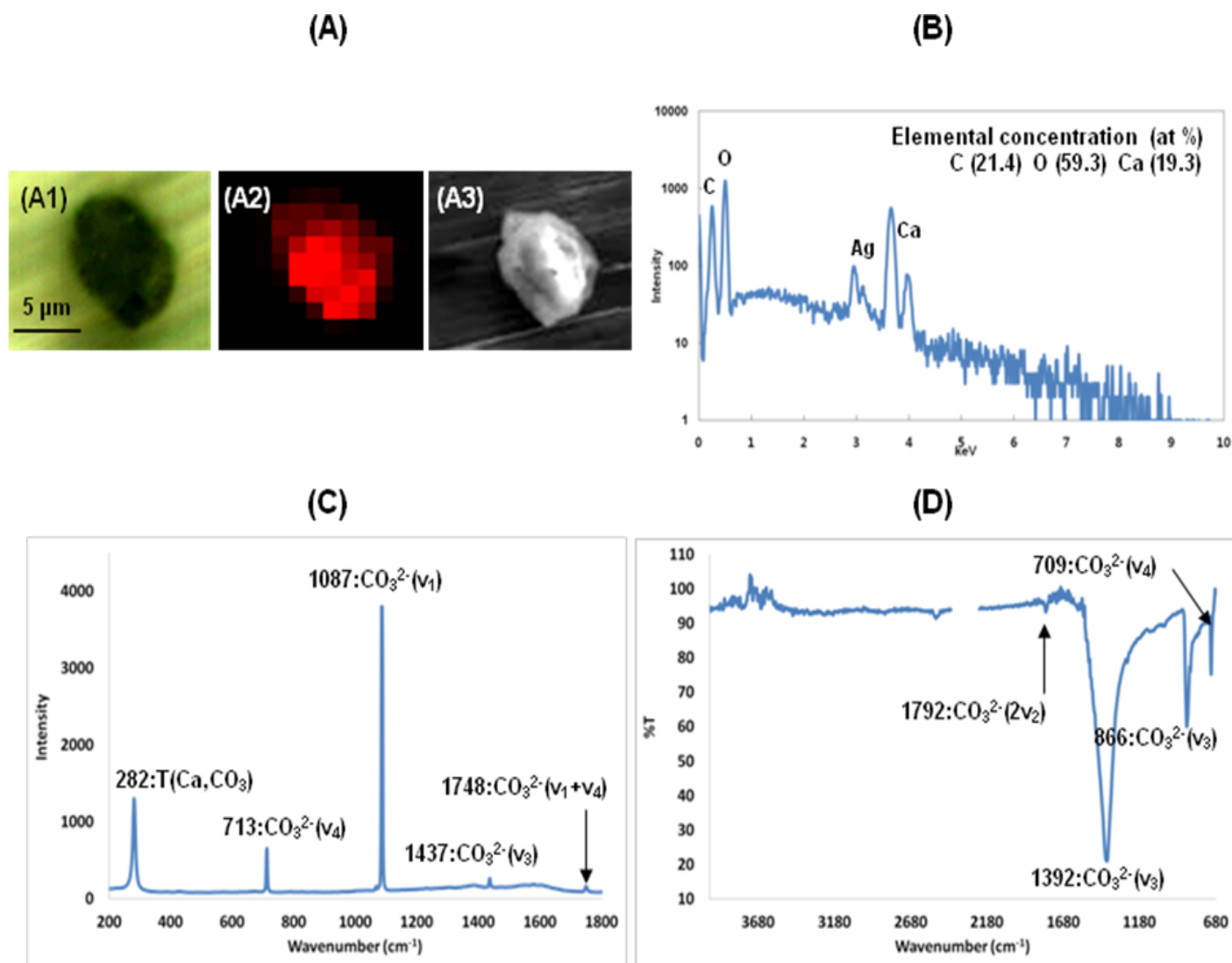


**Figure S4.** (A) SEI from SEM before ATR-FTIR measurement, (B) optical image from Raman spectrometer, (C) ATR-FTIR image at  $1060\text{ cm}^{-1}$ , and (D) SEI after ATR-FTIR measurement of the same 25 quartz particles on Ag foil.

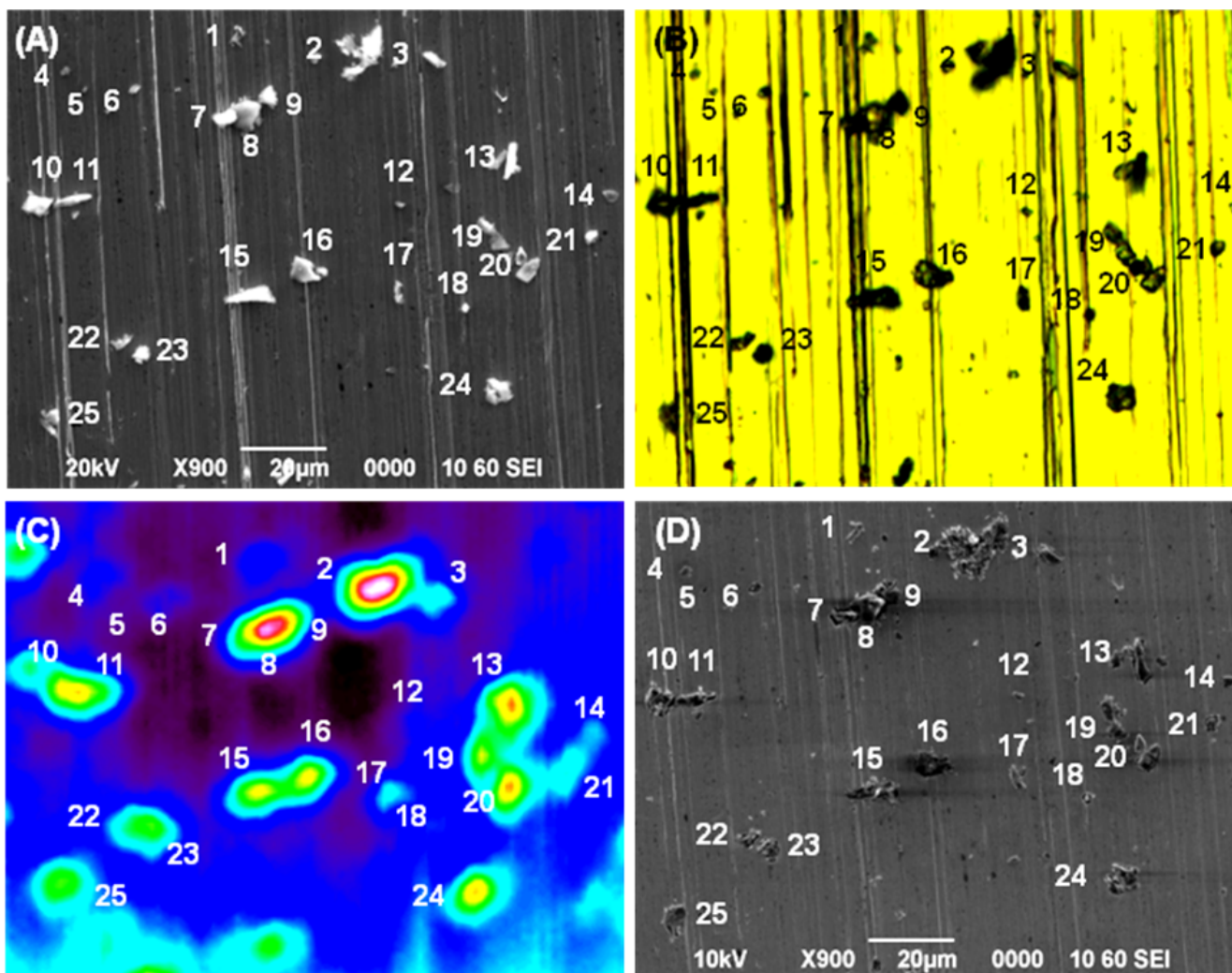


**Figure S5.** (A1) Optical image from Raman spectrometer, (A2) corresponding Raman image, and (A3) SEI of quartz particle #15, respectively, and (B) its X-ray spectrum, (C) Raman spectrum, and (D) ATR-FTIR spectrum.

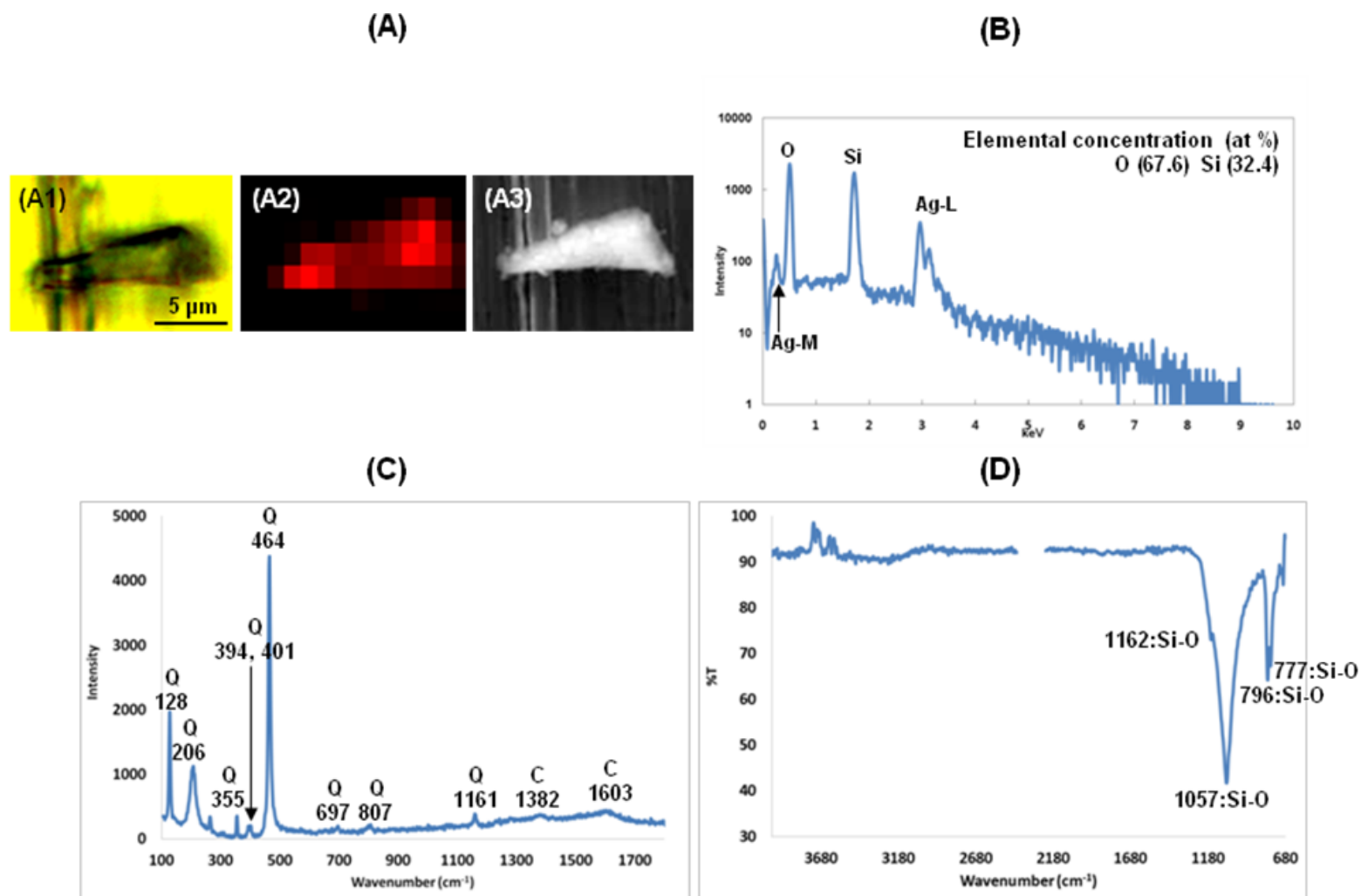




**Figure S6.** (A) SEI from SEM before ATR-FTIR measurement, (B) optical image from Raman spectrometer, (C) ATR-FTIR image at  $1100\text{ cm}^{-1}$ , and (D) SEI after ATR-FTIR measurement of the same 10 sodium sulfate particles on Al foil.

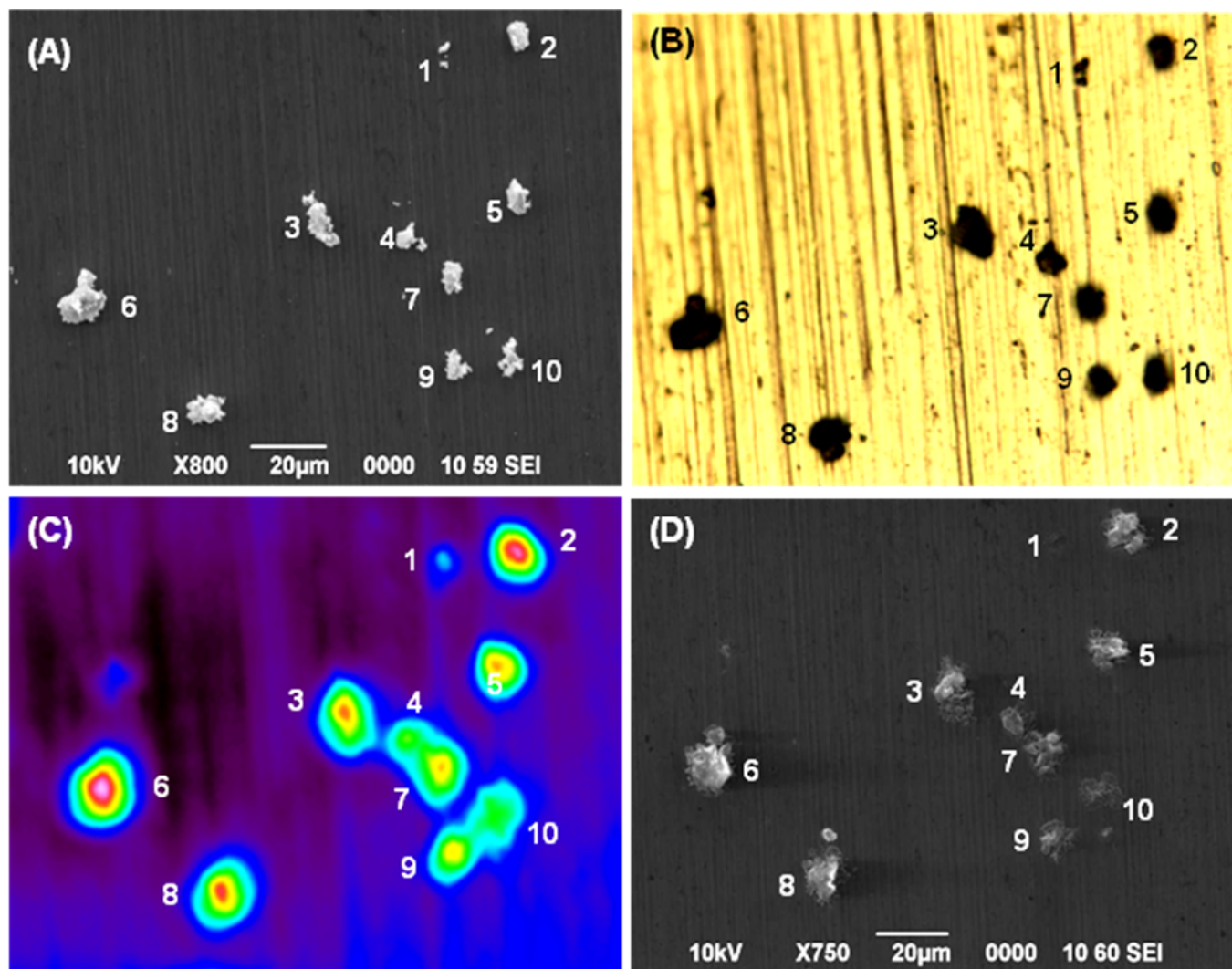


**Figure S7.** (A1) Optical image from Raman spectrometer, (A2) corresponding Raman image, and (A3) SEI of sodium sulfate particle #2, respectively, and (B) its X-ray spectrum, (C) Raman spectrum, and (D) ATR-FTIR spectrum.

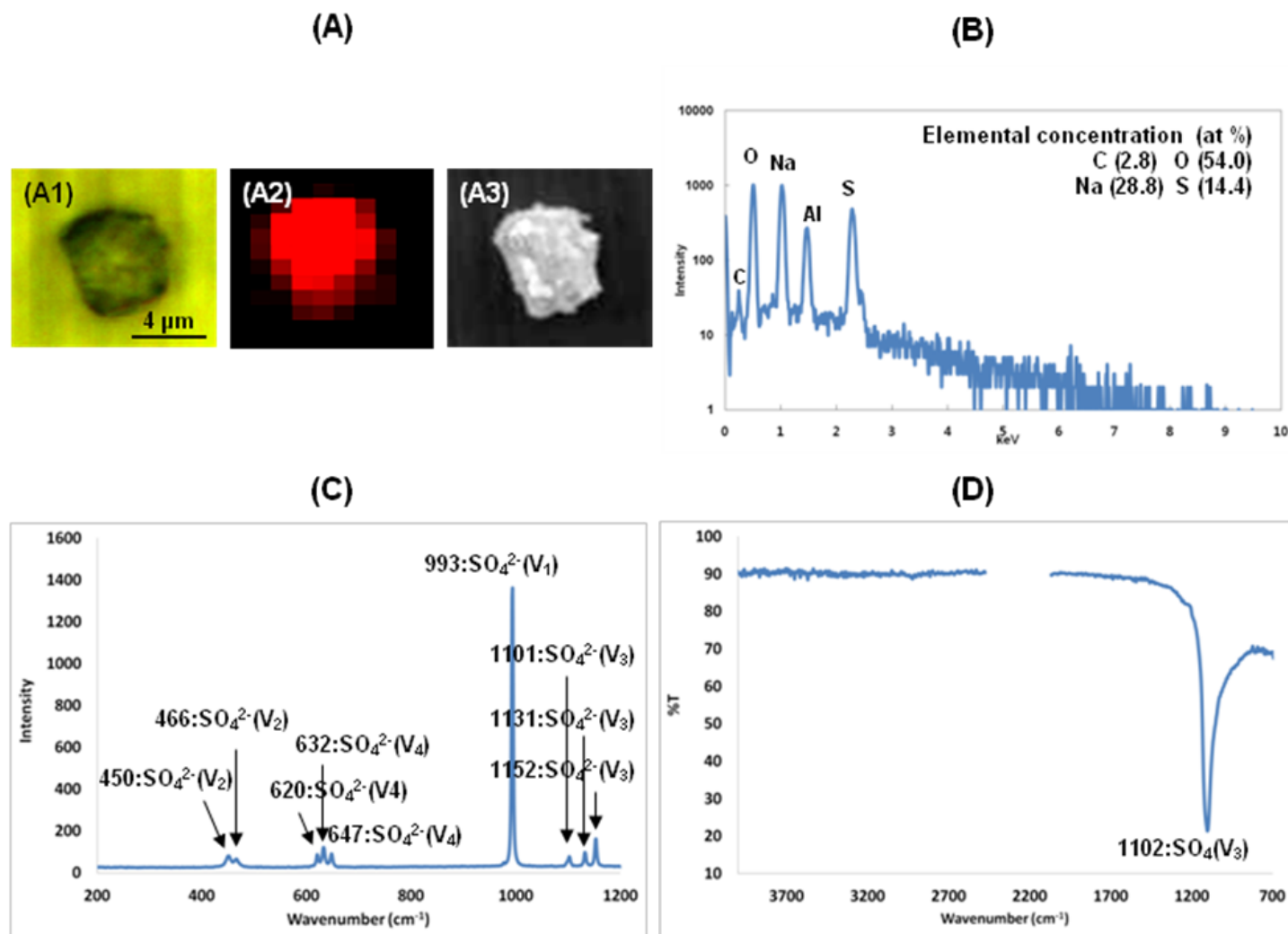


**Figure S8.** (A) SEI from SEM before ATR-FTIR measurement, (B) optical image from Raman spectrometer, (C) ATR-FTIR image at  $1350\text{ cm}^{-1}$ , and (D) SEI after ATR-FTIR measurement of the same 16 sodium nitrate particles on Al foil.

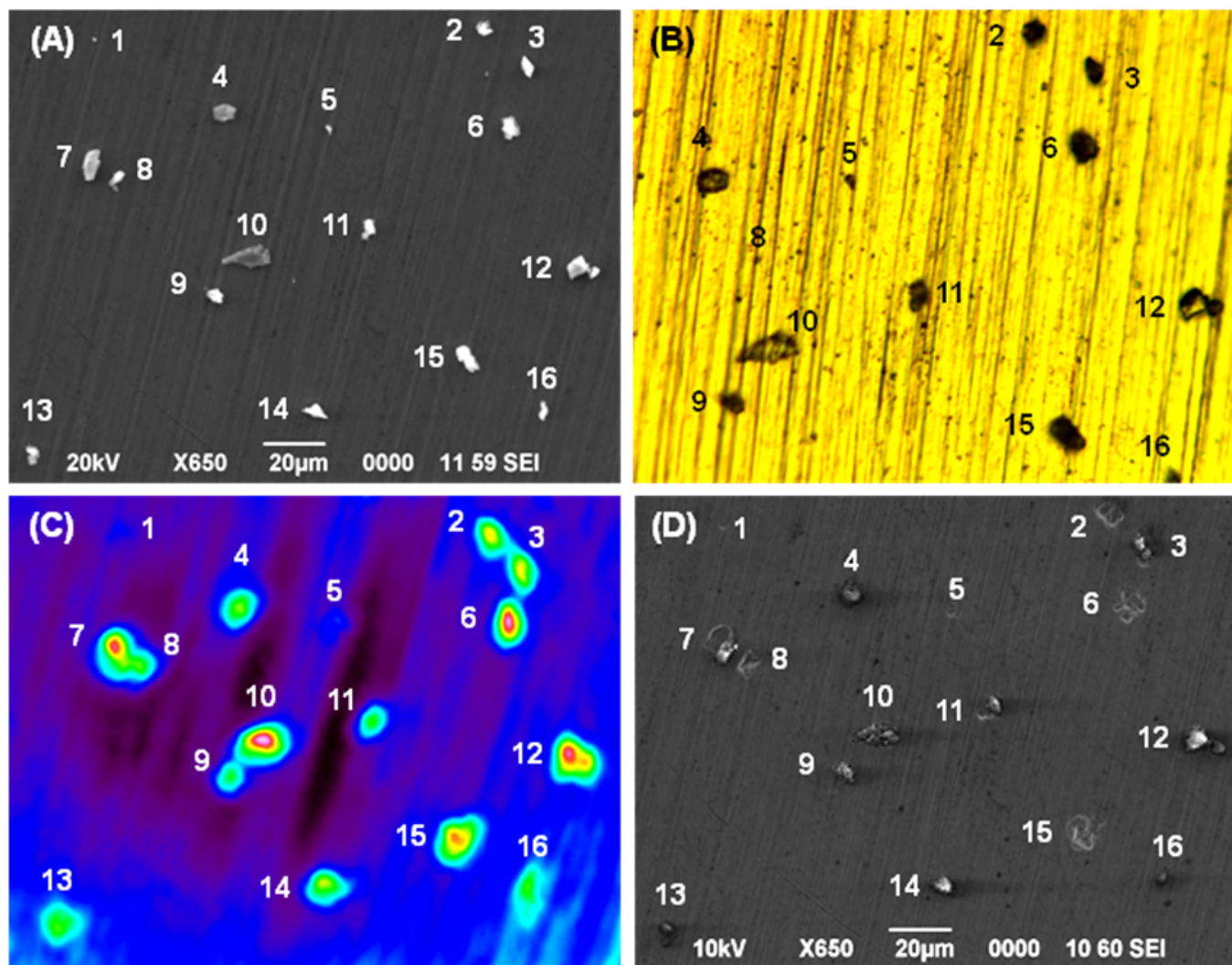


**Figure S9.** (A1) Optical image from Raman spectrometer, (A2) corresponding Raman image, and (A3) SEI of sodium nitrate particle #12, respectively, and (B) its X-ray spectrum, (C) Raman spectrum, and (D) ATR-FTIR spectrum.

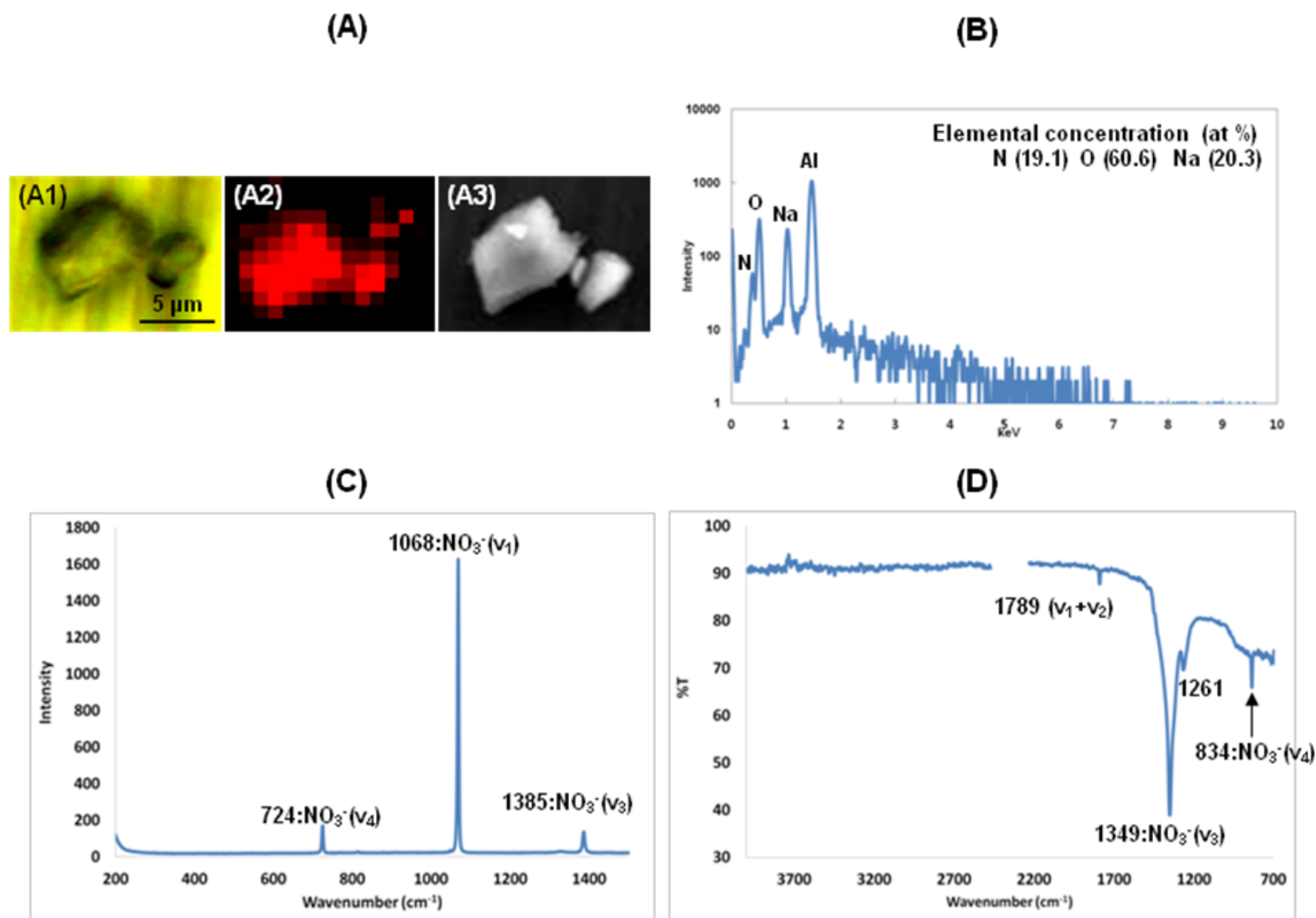


**Figure S10.** (A) SEI from SEM before ATR-FTIR measurement, (B) optical image from Raman spectrometer, (C) ATR-FTIR image at  $1010\text{ cm}^{-1}$ , and (D) SEI after ATR-FTIR measurement of the same 19 K-feldspar particles on Al foil.

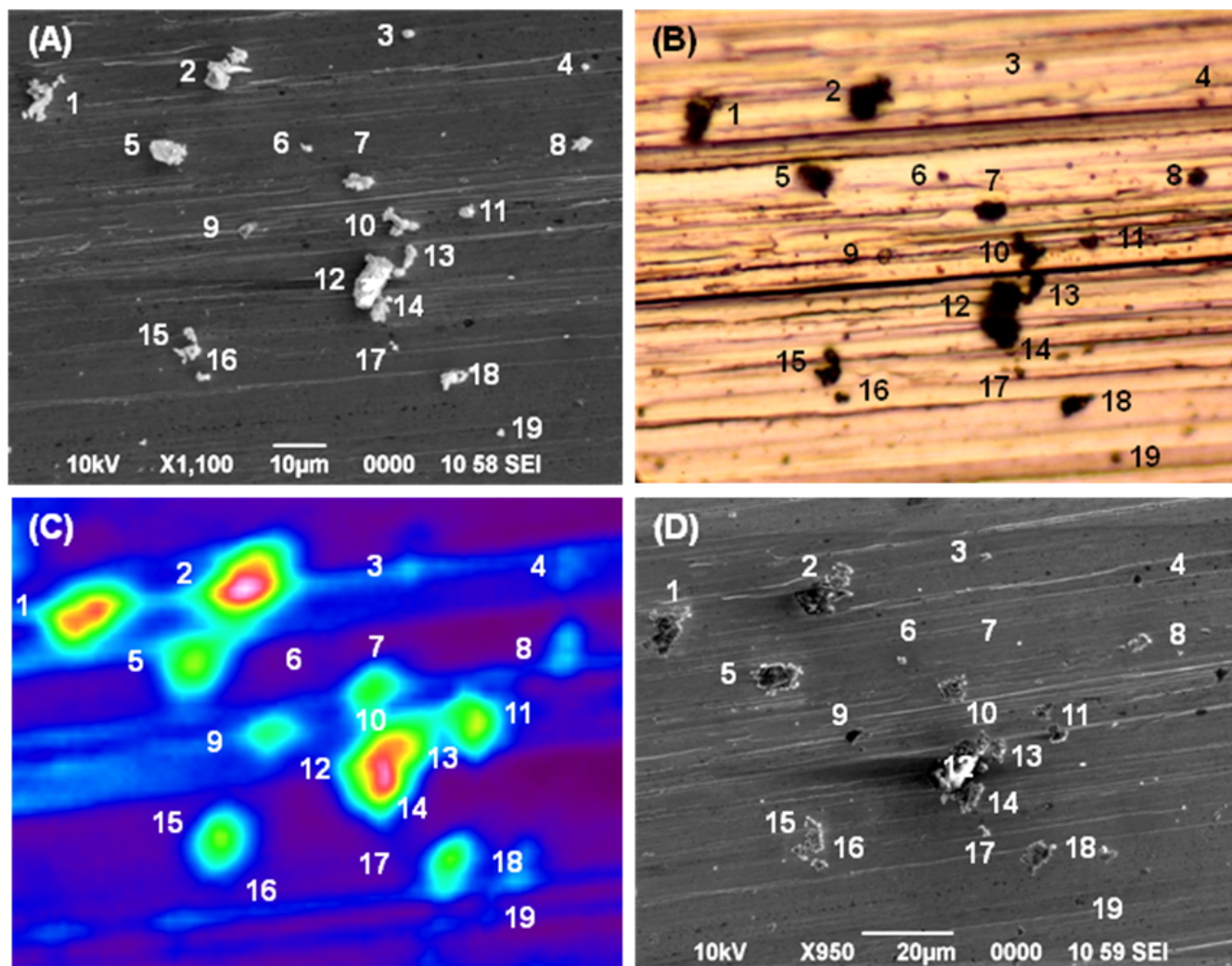


**Figure S11.** (A1) Optical image from Raman spectrometer, (A2) corresponding Raman image, and (A3) SEI of K-feldspar particle #15, respectively, and (B) its X-ray spectrum, (C) Raman spectrum, and (D) ATR-FTIR spectrum.

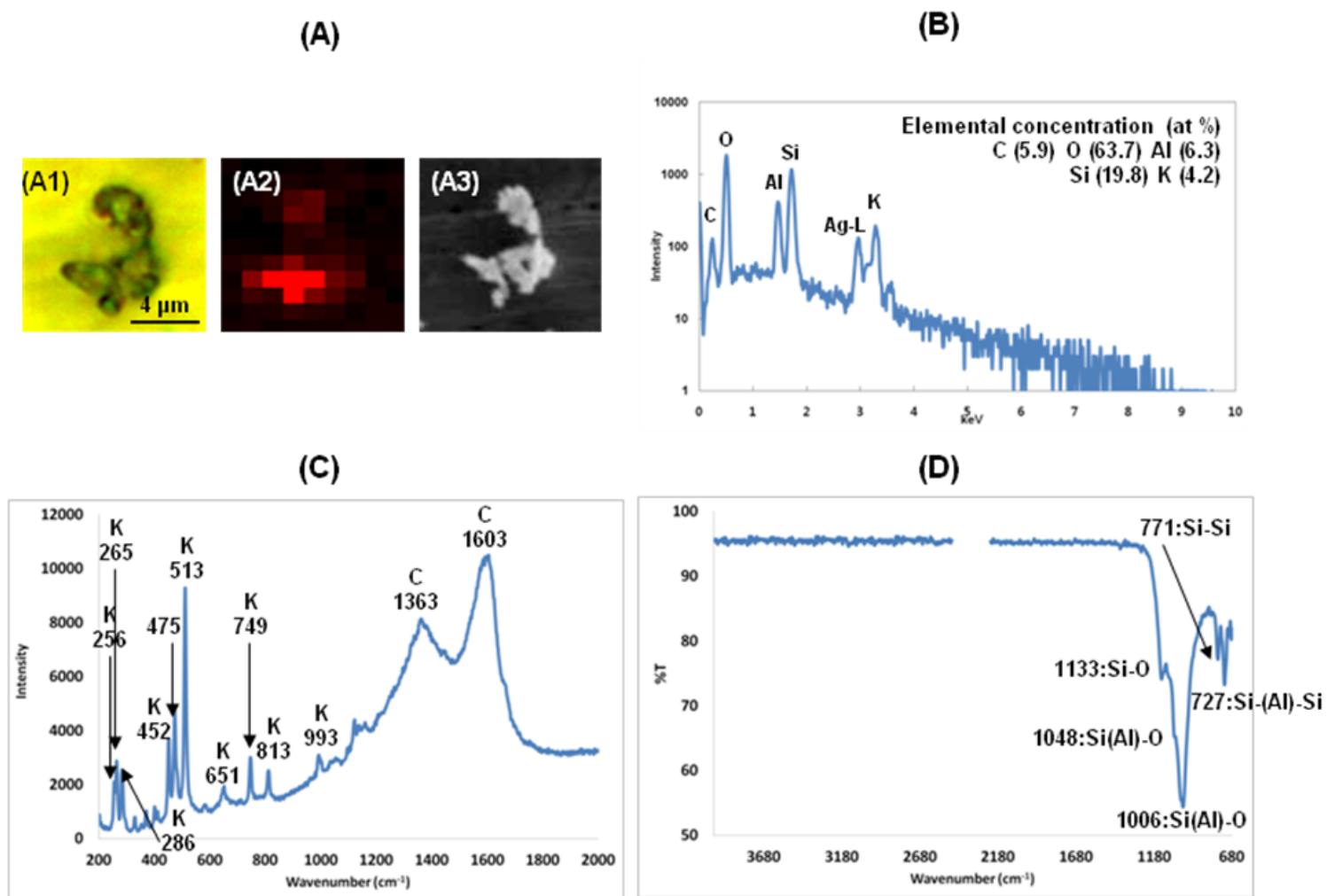


**Figure S12.** (A) Optical images from Raman spectrometer (A1), corresponding Raman images ((A2), (A3), and (A4)) of standard anhydrite particles #3 and #4, (B) ATR-FT-IR images ((B1) at 1090  $\text{cm}^{-1}$  and (B2) at 1400 $\text{cm}^{-1}$ ) of the anhydrite particles and (C) X-ray spectrum, (D) Raman spectra, and (E) ATR-FT-IR spectra of particle #4, respectively.

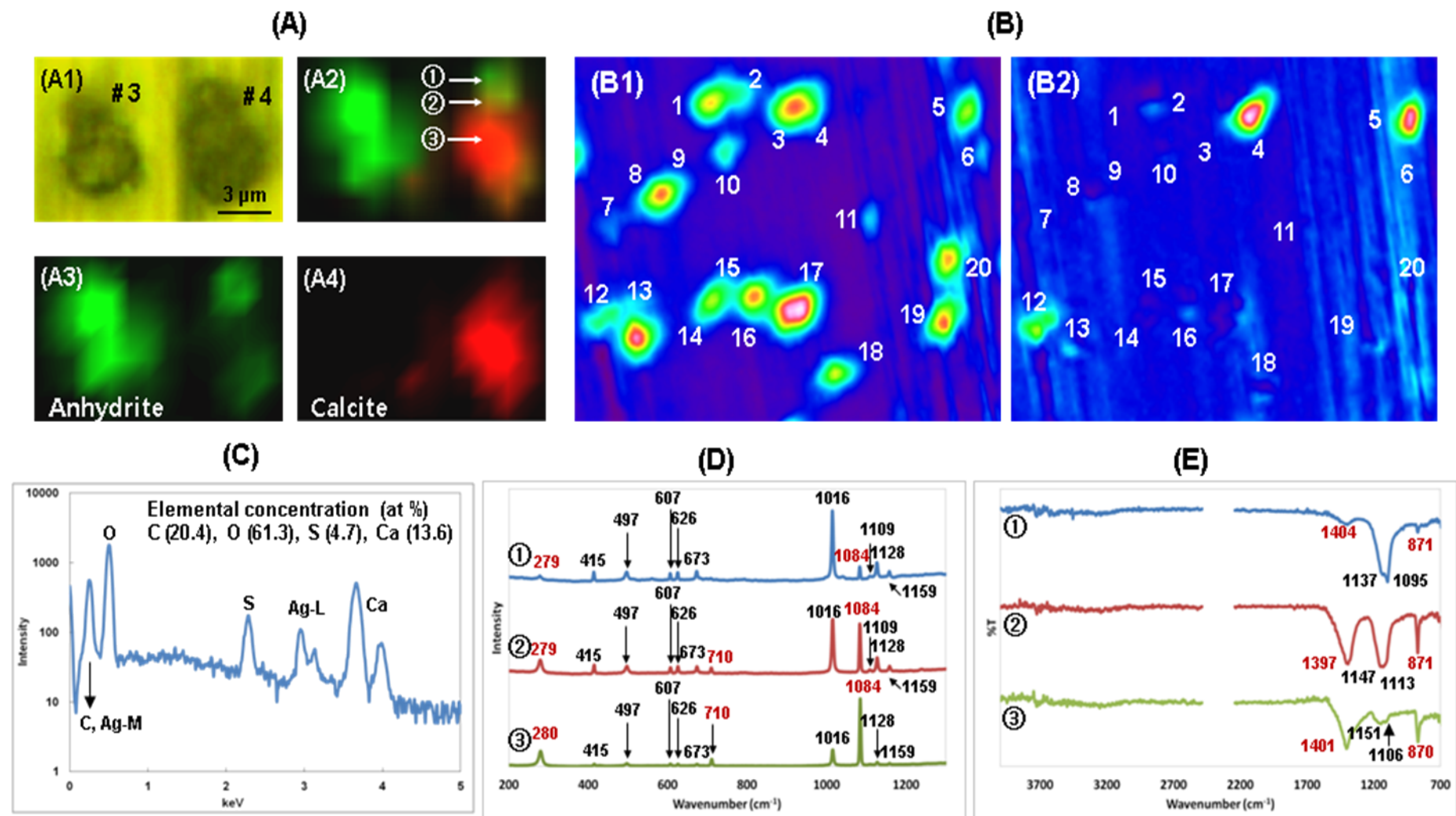


**Figure S13.** (A1) Optical image from Raman spectrometer, (A2) corresponding Raman image, and (A3) SEI of a gypsum particle (particle #9 in Figure S1) mixed with anhydrite, and (B) its X-ray spectrum, (C) Raman spectra, and (D) ATR-FTIR spectra.

